MEASUREMENT OF LOCAL BUBBLE DIAMETERS AND ANALYSIS OF GAS DISPERSION IN AN AERATED VESSEL WITH DISK-TURBINE IMPELLER

WEI-MING LU*, RUEY-CHI HSU, WEN-CHEN CHIEN AND LI-CHANG LIN

Department of Chemical Engineering, National Taiwan University, Taipei, Taiwan, R.O.C.

Key Words: Bubble Size Distribution, Bubble Size Measurement, Aerated Stirred Tank

An improved photoelectric capillary method was used to determine the characteristics of the gas dispersion in a stirred tank by disk-turbine impellers with various numbers of blades to examine the effect of the number of blades. The results show that the bubble size distribution in the system has three different characteristics according to the patterns of liquid flow. In the impeller discharge region the sizes of bubbles are dominated by the strength of the trailing vortex and the cavity structure behind the blades. No difference is observed among impellers with various numbers of blades when the region-averaged Sauter mean diameter $\overline{D_{32}}$ is correlated with P_g/V and Q_g.

In the upper circulation region, bubble size is affected by both the cavity structure and the circulating flow. In the lower circulation region, bubble size is controlled mainly by the pumping capacity of the impeller. These transitional rotation speeds, N_c and N_R, were obtained from the relationship between $\overline{D_{32}}$ and gas flow number Fl, which can serve not only as the turning points of the status of gas dispersion, but also can be used to explain the characteristics of the bubble size distributions for each region.

Introduction

Gas-liquid contact in agitated vessels is applied extensively in chemical and biological processes. One of the best-known devices is the disk-turbine impeller, which can provide a large interfacial area and shear stress. Many studies of physical aspects and mass transfer in such systems have been done in the past, but knowledge of how to design the systems optimally is still limited. To gain a better understanding of the phenomena of gas-liquid interaction in these systems, more detailed studies of the mechanism of gas dispersion and hydrodynamics of gas-liquid flow in the systems are required.

The stages of gas dispersion in an agitated vessel with Rushton turbine impeller have been studied extensively by Smith with his coworkers[3, 13, 18-21] and Nienow with his coworkers[11-13] in the past decades. The five stages of gas dispersion according to the characteristics of gas dispersion are presented by Nienow *et al.*[12] as shown in **Fig. 1**. They pointed out that most of the gas is drawn into the cavities behind the blades, and is then dispersed into small bubbles from the tip of the trailing vortex. Bruijn *et al.*[3] proposed that at a given rotational speed the cavity structure is transformed from a vortex cavity into a clinging cavity and then into a large cavity if gassing rates increased. Ismail and Nagase[7], Nienow *et al.*[12, 13] and Warmoeskerken[22] have concluded that the cavity structures reflected directly on the power consumption. Most previous studies were concentrated on six-blade impellers. A few papers, such as those of Bruijn *et al.*[3], Lu and Ju[10] Warmoeskerken[22] have reported on the characteristics of both power consumption and cavity formation behind the blades for a disk-turbine impeller with various numbers of blades.

Gaining a better knowledge of either overall bubble size or local bubble size distribution is the key to grasping the mass transfer rate or reaction rate in such an aerated agitated vessel. There are many methods for determinating the local bubble size in aerated stirred tanks[1, 2, 4-6, 8, 9, 12, 14-17, 23, 24]. Among them, the photoelectric capillary method developed by Weiland[23] is used very often in aerated stirred tanks[2, 5, 6, 23, 24]. Applying a high-speed data acquisition system, Greaves and Kobbacy[5] and Barigou and Greaves[2, 6] were able to measure local bubble sizes with excellent reproducibility. In discussing the problem of bubble breakage, Greaves and Kobbacy[5] proposed only an additional method to compensate the error due to the breakage of bubbles.

This paper presents a modified capillary probe method which concerns bubble breakage during the course of measurement. The method is applied to determine the local bubble size in an aerated vessel, and the measured bubble size distributions are used to analyze the characteristics of gas dispersion in an aerated stirred vessel by disk-turbine impellers with various numbers of blades.

1. Experimental

1.1 The stirred tank

* Received November 2, 1992. Correspondence concerning this article should be addressed to W.-M. Lu.

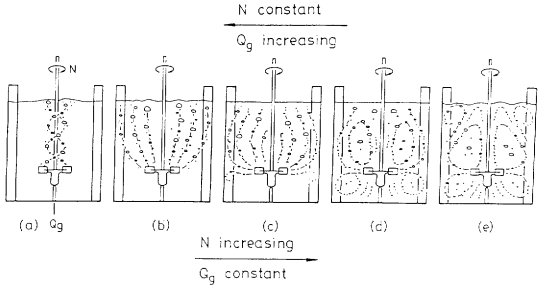

Fig. 1 The five characterisitc stages of gas dispersion defined by Nienow et al. (1977)
(a) partial bubble column
(b) full bubble column
(c) onset of dispersion into lower part
(d) complete circulation
(e) secondary circulation

Table 1. Comparison of experimental conditions

Experimental conditions	Nienow *et al.**	This work
Diameter T (m)	0.29	0.288
Liquid depth H	1 T	1.2 T
Impeller clearance ratio, h/T	1/4	1/3
Impeller/Tank ratio, D/T	1/8 to 3/4	1/3
Number of blades	6	4, 6, 8
Baffles (4 off)	0.1 T	0.1 T
Base	Flat	Flat
Sparger	Pipe point	Ring
Gassing rate $\times 10^5$ (m^3/s)	6.3-75	3.33-12.5
Rotational speed (rps)	1.2-21.7	4.17-8.33

* These experimental conditions were abstracted from Nienow *et al.*[12]

The investigation was carried out in a flat-bottomed transparent acrylic tank of which the major dimensions are given in **Table 1**. The disk-turbine impeller was 0.096 m (1/3 T) in diameter, with four, six or eight blades. The rotational speed and power consumption were measured with a photo-digital tachometer and a torsion angle type torque meter. Tap water and filtered air were used as the liquid and gas phases, respectively. Air was supplied from a ring sparger of 0.092 m diameter mounted 0.032 m (1/3 D) below the impeller disk and having twelve holes of 0.001 m diameter. A schematic diagram of the entire stirred tank system along with the bubble size measurement device is shown in **Fig. 2.**

1.2 The bubble size measuring device

The primary principle of the photoelectric capillary method is to use the difference in the intensities of light transmitted through gas and liquid when they are flowing through the capillary. The volume of the gas bubble is then evaluated from the length of slug formed by gas within the capillary. A Pyrex capillary tube, 0.8 mm ID and 0.7 m long and with a funnel-shaped suction probe of inner diameter 0.01 m to reduce the breakage of bubbles, was used as a sampling probe. The mixture of gas bubble and liquid at the measuring point was sucked into the probe under a constant vacuum (or pressure difference) through the capillary to the gas-liquid separator. A photodio (type TFK110-TCST2103) which consists of an infrared light emitter on one side of the tube and a light detector on the other was used to detect the intensity of the light transmitted through different fluids. The signal is amplified to a satisfactory value to differentiate easily whether the passing fluid is liquid or gas. To clarify the signal and to make the bubble counting easier, a comparator was adopted to adjust the signals to two set voltages. If the input signal was larger than a reference voltage, it was converted to 5.0 V; otherwise it was set to 0.0 V. The reference voltage was set to 2.0 V. The periodic time of pulses was determined by using two AX-5411 counter cards, one for gas and the other for liquid. The counters are operated at a speed of 1 MHz to reduce possible errors.

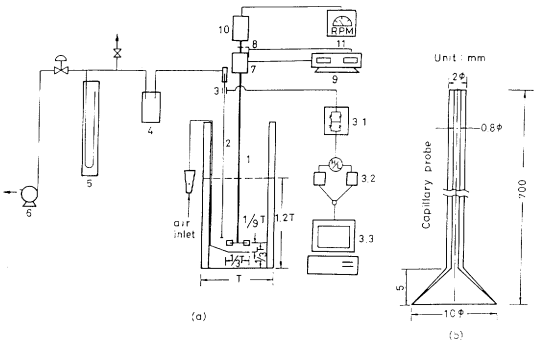

Fig. 2 Schematic flow diagram of the apparatus: (a) 1 stirred tank; 2 capillary 3 photodio; 3.1 amplify and comparator; 3.2 counter card; 3.3 286-AT PC; 4 vacuum jar; 5 mercury manometer; 6 vacuum pump; 7 torque detector; 8 speed detector; 9 torque and speed indicator; 10 DC motor; 11 speed controller. (b) capillary probe

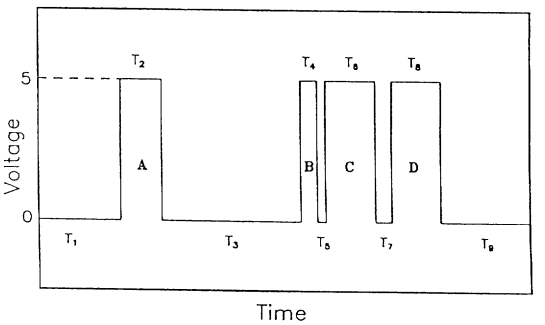

Fig. 3 Typical output signal of breakage bubbles

1.3 Processing algorithm

Bubble breakage at the entrance of the probe often occurs during the measurements, and causes erroneous interpretation of the signals. In **Fig. 3**, a typical signal output which contains a non-broken bubble (pulse A) and a broken bubble (combination of pulses B, C and D) is shown. The later signal actually represents a bubble's breakage into three small ones when it is sucked into the capillary. To avoid misinterpretation of the signals, a ref-

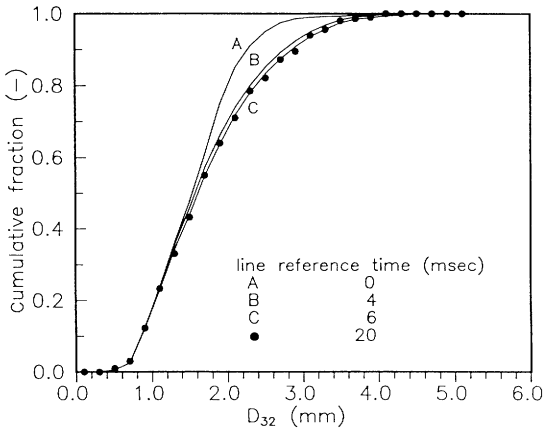

Fig. 4 A typical family of cumulation curves of bubble sizes for various reference times

erence periodic time was set to differentiate broken and non-broken bubbles.

To choose the reference time, a set of data taken at a sampling point are processed with several reference periodic times and the results are shown in the form of cumulative curves in **Fig. 4**. The curve A represents a result without taking into consideration the account of breakage of bubbles in data processing. This curve clearly indicates that if the broken bubbles are counted independently, it will result in a large amount of small bubbles. The curves B, C and solid circles represent the result of the data processed by considering the breakage with a reference periodic time of 4, 6 and 20 msec, respectively. No significant difference is seen if the reference time is larger than 6 msec; this rationalizes our choice of 6 msec as a reference periodic time. If the liquid pulse between two gas pulses was smaller than 6 msec, the volumes of bubbles would be added together and treated as that of a single bubble.

1.4 Calibration

In the calibration process, a series of calibrated needles were used to generate bubbles with various diameters ranging from 1.2 to 4.8×10^{-3} m. At a constant suction pressure, the lengths of periods generated by these gas slugs corresponded to the bubble volume. For each bubble size, 2000 bubbles were sampled and the averaged value was taken. Comparing the differences between the results of sucking a series of bubbles and sucking a single bubble, Barigou and Greaves[2] found the difference between them was less than 8 %. In our calibration, we chose to calibrate the bubble diameter under a condition closer to the experimental one. To avoid any misinterpretation of the signal, the breakage bubbles were discarded during the calibration process. Three pressure differences, i.e. 16, 20 and 22.7 kPa., were used. By considering the effects of breakage and interaction, the pressure difference of 20 kPa (150 mmHg) was used throughout this study.

1.5 The sampling points

In this study, all the measurements were conducted at the mid-plane (45°) which was centered between two

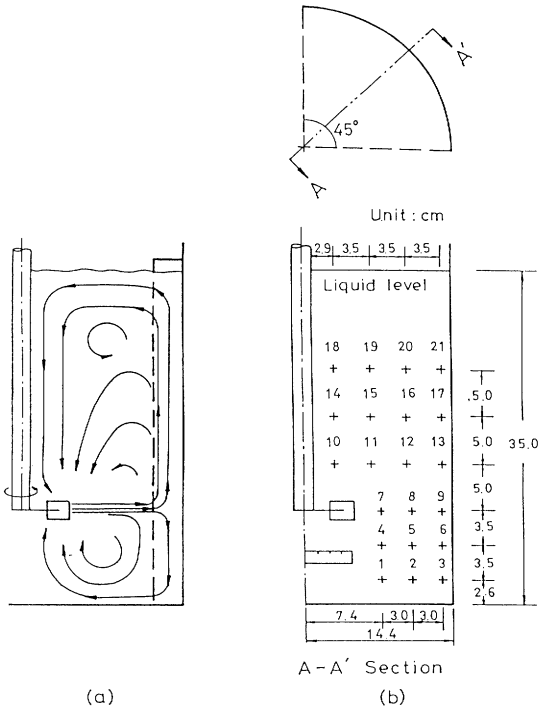

Fig. 5 (a) Three different liquid flow patterns; (b) measurement positions

baffles. Since there were three different flow patterns of liquids, i.e. the impeller discharge region, the upper circulation region and the lower circulation region, the 45° mid-plane was divided into three regions according to the liquid flow patterns and measurements were taken at 21 locations as shown in **Fig. 5**.

1.6 Definitions of local and region-averaged sauter mean diameters

The **local Sauter mean diameter** is defined as the time average size of the bubbles at a sampled point i and can be given as

$$D_{32,i} = \frac{\Sigma n_j D_j^3}{\Sigma n_j D_j^2} \tag{1}$$

where n_j is the number of the bubbles of D_j.

In each region, the **region-averaged Sauter mean diameter** is evaluated by considering both the frequency of bubbles and the volume of the representative zone for the sampling point and is defined as

$$\overline{D_{32}} = \frac{\Sigma D_{32,i} N_i V_i}{\Sigma N_i V_i} \tag{2}$$

where $D_{32,i}$ is D_{32} for the region i, N_i the number of bubbles measured in unit time, and V_i the regional volume of location i.

2. Results and Discussion

In this study, all the bubble sizes were determined under the conditions given in Table 1. The gassing rates (Q_g) and rotational speed (N) were set to provide the

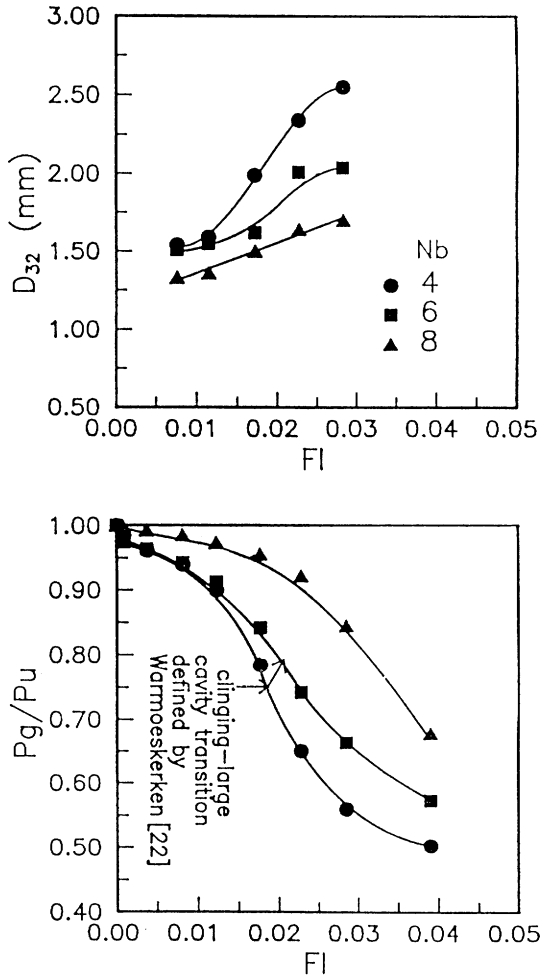

Fig. 6 D_{32} and Pg/P_u vs. Fl for various impellers at point 7 under N = 5 rps

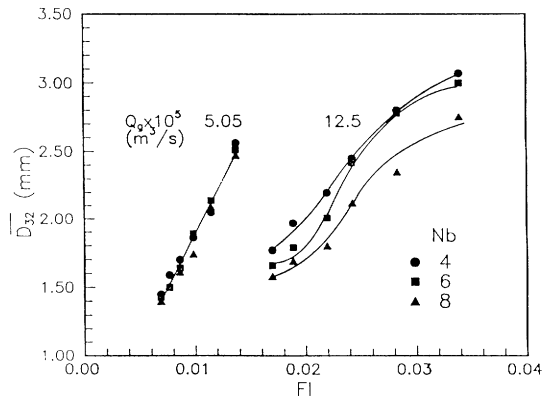

Fig. 7 $\overline{D_{32}}$ vs. Fl for various impellers in the impeller discharge region at various gassing rates

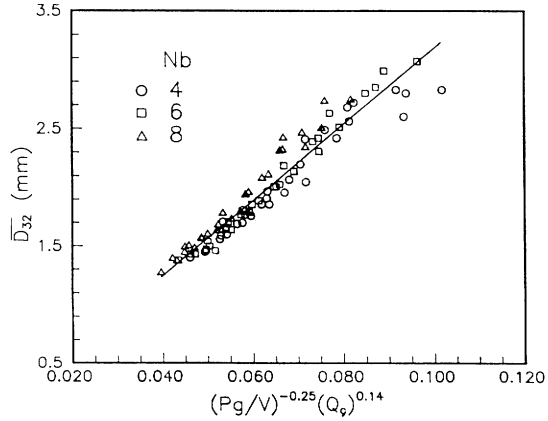

Fig. 8 $\overline{D_{32}}$ vs. $(Pg/V)^{-0.25}Q_g^{0.14}$ for all impellers in the impeller discharge region

status of gas dispersion from stage (*b*) to stage (*e*) as shown in Fig. 1. To avoid air entrainment from the surface, $H/T = 1.2$ was adopted.

Since the differences in fluid velocity and in flow pattern as shown in Fig. 5 in each flow region cause different characteristics in gas dispersion and coalescence, the results of bubble size measurement will be presented separately for each region.

2.1 The impeller discharge region

To examine how the Fl number (Qg/ND^3) and the number of blades (Nb) affect the dispersion of gas, the values of D_{32} at point 7 and the power consumed were determined for impellers with various Nb. Typical results for N = 5rps plotted against Fl are shown in **Fig. 6**. It is interesting to note that the point of inflection of the curve of D_{32} vs. Fl occurs almost at the same point of the transition from clinging cavity to the "3-3" large cavity for the case of Nb = 6 (i.e. for case of Nb = 4 the cavity status changes from clinging cavity to "2-2" large cavity) as in the plots of Pg/Pu vs. Fl which were defined by Warmoeskerken[22]. These results indicate that the cavity structure plays an important role in the size of the bubbles at this point. At this point, D_{32} was correlated with $\sigma^{0.6}/[(Pg/Vd)^{0.4}\rho^{0.2}]$ under different operating conditions, and the correlation is almost the same as the result of Parthasarthy[15] except that the slope is 1.96 instead of 2.0.

$\overline{D_{32}}$ for the impeller discharge region for impellers with various Nb and Qg are plotted against Fl in **Fig. 7**. The relationship between $\overline{D_{32}}$ and Fl is seen to be linear in the region of $Fl < 0.01$ or smaller Qg (i.e. 5.05×10^{-5} m³/s), and these straight lines coincide with each other regardless of the number of blades. Then the changes of $\overline{D_{32}}$ become an *S*-shape curve if Fl is beyond the value of 0.01 or larger Qg (i.e. 12.50×10^{-5} m³/s). These results seem to imply that the sizes of bubbles are dominated by the pumping capacity of the impeller if Qg values are not so large. Thus the bubble size is affected severely by the structure of the cavity behind the blade if Qg is large enough to overpass the transitional point of the cavity structure. In **Fig. 8**, $\overline{D_{32}}$ of the impeller discharge region was correlated with operating variables such as Pg/V and Qg in the range of our experimental conditions, listed in Table 1, and the result can be given as

$$\overline{D_{32}} = 33.4(P_g/V)^{-0.25}Qg^{0.14} \quad (3)$$

regardless of the number of blades.

2.2 The upper circulation region

To analyze how the pumping capacity of the impeller will affect the average $\overline{D_{32}}$ over the upper cir-

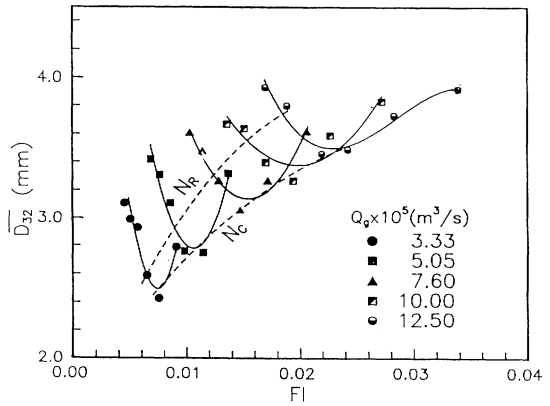

Fig. 9 $\overline{D_{32}}$ vs. *Fl* for *Nb* = 4 in the upper circulation region at various gassing rates

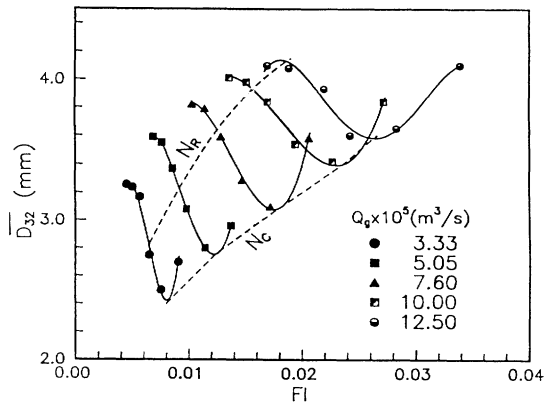

Fig. 10 $\overline{D_{32}}$ vs. *Fl* for *Nb* = 6 in the upper circulation region at various gassing rates

culation region, the relationship between $\overline{D_{32}}$ and *Fl* for impellers with various *Nb* and *Qg* is shown in **Figs. 9, 10** and **11**. At a given *Qg*, $\overline{D_{32}}$ first decreases to a minimum value as *Fl* decreases (that is, increases in *N*), then increases to higher value as *N* continuously increases when the impellers have four and six blades. This fact demonstrates that if the value of *N* is smaller than that corresponding to the minimum $\overline{D_{32}}$, the negative pressure generated behind the blade is not strong enough to capture all the sparged gas, and the pumping capacity of the impeller is not high enough to create recirculation of the dispersed bubbles. Thus the most dispersed bubbles rise directly to the free surface. Consequently, the bubble sizes at this stage are dominated by the dispersion ability of the impeller, and the value of $\overline{D_{32}}$ decreases as *N* increases. As observed, this status of gas dispersion is within stage (b) and stage (c) as shown in Fig. 1. If the value of *N* is larger than the value of *N* corresponding to the minimum $\overline{D_{32}}$, the pumping capacity of the impeller will reach a value to at which stronger circulation of both liquid and gas is generated,whose flow pattern corresponds to stage (d) in Fig. 1. Thus the size of the bubbles will increase because the circulation of bubbles will enhance their coalescence. From the description given here, it is seen that the value of the rotational speed corresponding to the minimum $\overline{D_{32}}$ appearing in the plots

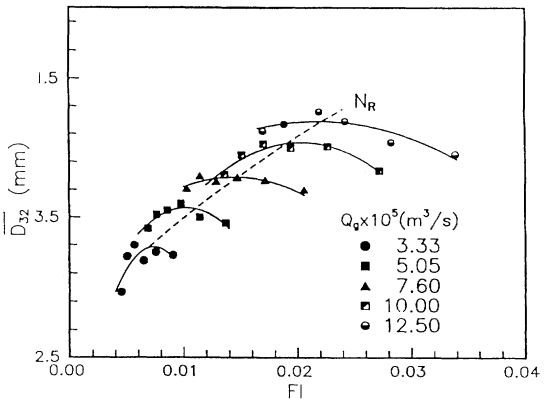

Fig. 11 $\overline{D_{32}}$ vs. *Fl* for *Nb* = 8 in the upper circulation region at various gassing rates

Table 2. Comparison of transitional speed for gas dispersion stage (c) to stage (d) in Fig. 1

$Qg \times 10^5$ m³/s	3.33	5.05	7.60	10.00	12.50
N_{cd} (rps)	1.383	2.25	2.75	3.17	3.53
N_c (rps)	4.70	4.75	5.12	5.18	5.63

N_{cd}: $Fl = 0.20\ (D/T)^{0.5}\ (Fr)^{0.5}$ defined by Nienow *et al.*[12]

N_c: defined in this study

of $\overline{D_{32}}$ vs. *Fl* is a transition speed at which the status of gas dispersion of the system shifts from stage (c) to stage (d) and can be defined as N_c. Due to the circulation flow of fluid, the major control factor for the size of bubbles in this region will be changed from gas dispersion by impeller to the degree of coalescence.

The values of N_c defined here are quite different from the values of N_{cd} proposed by Nienow *et al.*[12] as shown in **Table 2**. The difference is probably caused by the difference in layout of the impeller and design of the spargers as shown in Table 1.

Under our experimental conditions, the characteristics of gas dispersion of the eight-blade impeller system has overpassed stage (c); i.e. most data are beyond stage (d), and the curves of $\overline{D_{32}}$ vs. *Fl* show a different trend if they are compared with the plots of the four- and six-blade impellers. At a given *Qg*, $\overline{D_{32}}$ in smaller *N* or a larger value of *Fl* tends to increase to a maximum value, then to decrease as *N* increases. Comparing this result with the relationship between *Pg/Pu* and *Fl*, it is noted that the maximum $\overline{D_{32}}$ is found near the other transition point, N_R, a recirculation point defined by Nienow *et. al.*[12] (i.e. the transition point from stage (d) to stage (e) in Fig. 1) Fig.11, N_R lines are also given in Fig. 9 and 10. Therefore the change of $\overline{D_{32}}$ in this region at a given *Qg* can be explained as that, even at the lower *N*, the eight-blade impeller still pumps enough fluid to provide a circulatory flow, which can provide $\overline{D_{32}}$ up to the maximum value. When the increase of *N* goes beyond the maximum $\overline{D_{32}}$ or the point of N_R, part of the recycle bubbles are sucked into

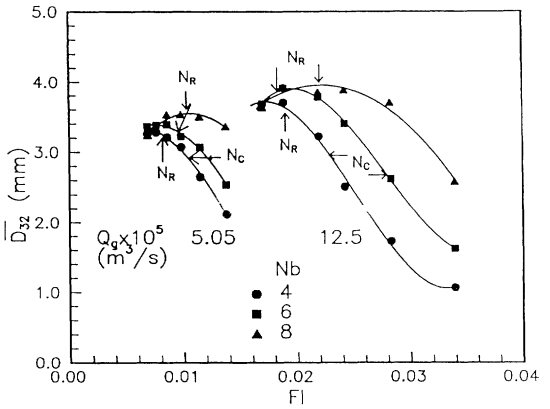

Fig. 12 $\overline{D_{32}}$ vs. Fl for various impellers in the lower circulation region at various gassing rates

the impeller and redispersed by the impellers which reduce $\overline{D_{32}}$. Therefore, the mechanism of gas dispersion by the trailing vortex again controls the size of bubbles.

2.3 The lower circulation region

Since bubbles scarcely appear in this region until the status of gas dispersion reaches stage (c) shown in Fig. 1, only smaller bubbles can be seen at lower N. To examine the role of recirculation in bubble-size distribution in this region, plots of $\overline{D_{32}}$ vs. Fl determined for this region are shown in **Fig. 12**. For a given Qg and lower N, the increase in N provides a stronger recirculation of fluids which enhances the coalescence of the bubbles; thus $\overline{D_{32}}$ increases to a maximum value. Beyond this maximum point, $\overline{D_{32}}$ will decrease because when N increases, the enhanced circulation flow will promote redispersion of bubbles by the impeller. These trends coincide with the results of Zhang *et al.*[24] Therefore the bubble sizes in this region are dominated by the strength of the circulation of fluid, and N_R corresponding to the maximum $\overline{D_{32}}$ can be seen as a transitional speed of the gas dispersion from stage (d) to (e) shown in Fig. 1.

The effect of the number of blades on $\overline{D_{32}}$ in this region can only be seen from the different pumping capacity of each impeller. The impeller with more blades shows stronger recirculation under the impeller, which results in the appearance of larger bubbles.

Conclusions

By taking into account the phenomena of bubble breakage in the sampling probe, an improved algorithm was designed to modify the photoelectric capillary method, which was then applied to determine the local bubble sizes in a 0.288 m flat-bottom cylindrical agitated vessel.

The results of the local bubble-size measurements show that the bubble size in an aerated agitated vessel is affected by the characteristics of the impeller as well as the flow patterns of liquid which are created by the pumped fluid. Three different types of bubble-size distributions are observed according to their flow patterns: the impeller discharge region, the upper circulation region and the lower circulation region.

In the impeller discharge region, both D_{32} and $\overline{D_{32}}$ are mainly controlled by the structure of the cavities. Under the conditions that $Qg = 3.33 - 12.5 \times 10^{-5}$ m³/s and $N = 4.17 - 8.33$ rps, almost no difference is found among various Nb if the values of $\overline{D_{32}}$ are correlated against (Pg/V) and gas flowrate Qg.

In the upper circulation region, a transitional speed of the impeller, N_c, is observed from the minimum point appearing in the plot of $\overline{D_{32}}$ vs. Fl at a constant Qg. At a given Qg, if $N > N_c$, the size of bubble is controlled by the structure of cavities. If $N_R > N > N_c$, both the intensity of gas dispersion and liquid flow control. When $N > N_R$, part of the recirculated gas is redispersed through the impeller, and thus the intensity of gas dispersion becomes the major control.

In the lower circulation region, the bubble size is mainly controlled by the pumping capacity of the impeller and the rotaional speed of N_R becomes a turning point. When $N > N_R$, the sizes are controlled by the gas dispersion, and if $N < N_R$, the pumping flow enhances the coalescence.

Acknowledgement

The authors wish to express their sincere appreciation to the National Science Council of R.O.C. for its financial support.

Nomenclature

D	=	impeller diameter	[m]
D_i	=	bubble size defined in eq. 2	[m]
D_{32}	=	Sauter mean bubble diameter	[m]
$\overline{D_{32}}$	=	region-averaged Sauter mean bubble diameter	[m]
Fl	=	gas flow number Qg/ND^3	[-]
Fr	=	Froud number N^2D/g	[-]
h	=	impeller clearance above the bottom	[m]
H	=	liquid depth N	[m]
N	=	rotational speed	[s⁻¹]
Nb	=	numbers of blades	[-]
N_c	=	transitional speed for stage (c) to stage (d) in Fig. 1 defined by this study	[s⁻¹]
N_{cd}	=	transitional speed for stage (c) to stage (d) in Fig. 1 defined by Nienow *et al.*[12]	[s⁻¹]
N_i	=	Frequency of bubbles used in eq. 3	[s⁻¹]
N_R	=	secondary recirculation speed	[s⁻¹]
P_g	=	gassed power consumption	[W]
P_u	=	ungassed power consumption	[W]
Q_g	=	gassing rate	[m³/s]
T	=	diameter of the tank	[m]
V	=	liquid volume	[m³]
V_d	=	impeller swept volume per revolution	[m³]
ρ	=	density	[kg/m]
σ	=	surface tension	[N/m]

Literature Cited

1) Bakker, A: Ph. D.Dissertation, Delft Univ. of Technology, Delft, Netherlands (1992)
2) Barigou M. and M. Greaves: *Meas. Sci. Technol.* **2,** 318 (1991)
3) Bruijn, W., Van't Riet, K. and J.M. Smith: *Trans. Instn. Chem. Engrs.*, **52,** 88 (1974)
4) Calderbank. P.H.: *Trans. Instn. Chem. Engrs.*, **36,** 443 (1958)
5) Greaves, M. and K.A.H. Kobbacy: *Chem. Eng. Req. Des.*, **62,** 3 (1984)
6) Greaves, M. and M. Barigou: Proc. 6th Euro. Conf. Mxing,

Pavia, Italy, 313 (1988).
7) Ismail, A.F.Y. and J.I. Nagase: *AIChE J.*, **30,** 487 (1984)
8) Kamiwano, M., M. Kaminoyama and K. Arai: Proc. ChIChE-SCEJ Joint Seminar on Mixing Technol., Taipei, Taiwan, 27 (1992)
9) Lopesde Figueiredo, M.M. and P.H. Calderbank: *Chem. Eng. Sci.*, **34,** 1333 (1979)
10) Lu W.M. and S.J. Ju: *Chem. Eng. Sci.*, **44,** 333 (1989)
11) Nienow, A.W. and D.J. Wisdom: *Chem. Eng. Sci.*, **29,** 1994 (1974)
12) Nienow, A.W., D.J., Wisdom and J.C., Middleton: 2nd Euro. Conf. Mixing, Cambridge, England, F1-1 (1977)
13) Nienow, A.W., M.M.C.G. Warmoeskerken, J.M. Smith and M. Konno: Proc. 5th Euro. Conf. on Mixing, Wurzburg, West Germany, 143 (1985)
14) Nagase, Y. and H. Yasui: *Chem. Eng. J.*, **27,** 37 (1983)
15) Parthasarathy, R., G.J. Jameson and N. Ahmed: *Trans. Instn. Chem. Engrs.*, **69,** 295 (1991)
16) Rennie, J. and F.H.H. Valentin: *Chem. Eng. Sci.*, **23,** 663 (1968)
17) Takahashi, K., W.J. McManamey and A.W. Nienow: *J. Chem. Eng. Japan,* **25 (4),** 427 (1992)
18) Van't Riet, K. and J.M. Smith: *Chem. Eng. Sci.*, **28,** 1031 (1973)
19) Van't Riet, K. and J.M. Smith: *Chem. Eng. Sci.*, **30,** 1093 (1975)
20) Vant' Riet, K., J.M. Boom and J.M. Smith: *Trans. Instn. Chem. Engrs.*, **54,** 124 (1976)
21) Warmoeskerken, M.M.C.G. and J.M. Smith: *Chem. Eng. Sci.*, **40,** 2063 (1985)
22) Warmoeskerken, M.M.C.G.: Ph. D. Dissertation, Delft Univ. of Technology, Delft, Netherlands (1986)
23) Weiland, P.: *Ger. Chem. Eng.*, **3,** 296 (1980)
24) Zhang, Z.B., G. Dai and M.H. Chen: *J. Chem. Ind. Engrs. China,* **2,** 183 (1989) (in Chinese)